Nano Energy 34 (2017) 399–407

Contents lists available at ScienceDirect

Nano Energy

journal homepage: www.elsevier.com/locate/nanoen

Full paper

Decoupling atomic-layer-deposition ultrafine RuO_2 for high-efficiency and ultralong-life Li-O_2 batteries

Changtai Zhao[a,b,1], Chang Yu[b,1], Mohammad Norouzi Banis[a], Qian Sun[a], Mengdi Zhang[b], Xia Li[a], Yulong Liu[a], Yang Zhao[a], Huawei Huang[b], Shaofeng Li[b], Xiaotong Han[b], Biwei Xiao[a], Zhongxin Song[a], Ruying Li[a], Jieshan Qiu[b,*], Xueliang Sun[a,*]

[a] Department of Mechanical and Materials Engineering, University of Western Ontario, London, ON, Canada N6A 5B9
[b] State Key Lab of Fine Chemicals, Liaoning Key Lab for Energy Materials and Chemical Engineering, PSU-DUT Joint Center for Energy Research, School of Chemical Engineering, Dalian University of Technology, Dalian 116024, PR China

ARTICLE INFO

Keywords:
Li-O_2 batteries
RuO_2
Atomic layer deposition
Long cycle life
High temperature

ABSTRACT

Li-O_2 batteries with ultrahigh theoretical energy density have triggered worldwide research interests and hold the prospect for powering electric vehicles. However, the poor cycling stability and low energy efficiency of Li-O_2 batteries still remain and hamper their practical application. Configuring desirable porous cathodes with uniformly dispersed and highly active catalysts is a noteworthy and feasible approach to overcoming these critical obstacles. Herein, we report on a novel strategy for the fabrication of Mn_3O_4 nanowires and carbon nanotubes composite film (Mn_3O_4/CNTs film) with ultrafine RuO_2 nanoparticles (Mn_3O_4/CNTs-RuO_2 film), in which the Mn_3O_4/CNTs film was employed as a conductive and porous matrix and extremely low amount of RuO_2 (just 2.84 wt%) are uniformly dispersed onto this matrix by using atomic layer deposition method, and reveal its electrochemical behaviors as a free-standing air electrode for Li-O_2 batteries. The Mn_3O_4/CNTs-RuO_2 film delivers a high specific capacity, improved round-trip energy efficiency and ultra-long cycle life (251 cycles). The superior electrochemical performance can be attributed to the enhanced catalytic activity of the grafted RuO_2 with modulated electronic structure as the result of the interaction with substrate, which is evidenced by the corresponding X-ray absorption spectroscopy results and the unique nanosheet-shaped discharge product which can be smoothly decomposed.

1. Introduction

The growing energy demand and the increasing concerns regarding the efficient utilization of sustainable energy resources have triggered worldwide research interests in the field of high-energy density and high-efficiency energy conversion and storage devices [1,2]. Li-O_2 batteries, with an ultrahigh theoretical energy density of 3500 W h kg^{-1}, have attracted tremendous attention because of their potential and promising application for driving electric vehicles (EVs) [3,4]. Nevertheless, there are still some remaining challenges in the practical application of Li-O_2 batteries, especially, the low energy efficiency and poor cycling stability that are continuously of concern and urgently need to overcome [5–7]. These critical issues are indeed associated with the formation and decomposition of the discharge product with low electronic conductivity in the air electrode [8,9]. One option to tackle these issues is to configure the state-of-the-art cathodes integrating all benefits such as advanced pore structure, excellent conductivity and highly efficient catalytic activity [10–12]. The electrode materials featuring the interconnected and porous structure and high conductivity can enable fast supply and transportation of O_2, Li ions and electrons [13–17]. But beyond that, an efficient catalyst is highly of concern and sought after for facilitating the terribly sluggish kinetics of oxygen evolution reaction (OER) process induced by the tough decomposition of the insulating and insoluble discharge product in the air electrode [18–22]. In response, various electrocatalysts, such as transition metal oxides, noble metals, and soluble redox mediators etc., have been developed and investigated in Li-O_2 batteries [23–28]. Among all of the candidates explored up to now, RuO_2 has demonstrated excellent electro-catalytic performance in terms of low overpotential and long cycle life [29–34]. Nevertheless, considering that Ru is a kind of scarce and costly metal, it is crucially important for reducing its dosage and fully fulfilling its efficacy or

* Corresponding authors.
E-mail addresses: jqiu@dlut.edu.cn (J. Qiu), xsun9@uwo.ca (X. Sun).
[1] The first two authors contributed equally to this work.

http://dx.doi.org/10.1016/j.nanoen.2017.02.030
Received 15 January 2017; Received in revised form 16 February 2017; Accepted 17 February 2017
Available online 20 February 2017

further enhancing its efficacy [35,36]. One of the great challenges is how to finely design and tune the micro-structure of this kind of catalyst to meet these requirements.

Atomic layer deposition (ALD) is a promising technique to precisely control the deposition of metal catalysts on various functional substrates. The chemical bonds formed between the initial layer atoms of a reactive species and the surface of support during its first cycle can ensure a strong interaction between the deposited material and support [37]. So ALD may offer a simple yet effective approach to the precise deposition of RuO_2 catalyst with uniform distribution and controllable loading and particle size [38]. Meanwhile, an appropriate substrate can be used as the promoter for enhancing the catalytic activity of RuO_2 due to the strong interaction between them. Therefore, the precisely controllable deposition of RuO_2 catalyst on advanced porous electrode by ALD may offer an effective approach to substantially enhance the electrochemical performance of Li-O_2 batteries.

Herein, we present a simple yet effective strategy for the self-assembly of Mn_3O_4 nanowires and carbon nanotubes (CNTs) composite film (Mn_3O_4/CNTs film) as a free-standing substrate for the uniform deposition of extremely low amount of RuO_2 nanoparticles (just 2.84 wt%) (Mn_3O_4/CNTs-RuO_2 film), and demonstrate its electrochemical performance as a highly efficient air electrode for Li-O_2 batteries. In the composite film, the Mn_3O_4 nanowires function as skeletons for constructing interconnected channels, CNTs as good conductors contribute to the high conductivity, and the uniformly dispersed and ultrafine RuO_2 nanoparticles on Mn_3O_4 nanowires made by ALD process as the highly effective catalyst are responsible for the smooth decomposition of the discharge product. Benefiting from these combined structure and composition merits, the as-made Mn_3O_4/CNTs-RuO_2 film delivers a high specific capacity, low overpotential, and long cycle stability up to 251 cycles as a binder-free air electrode for Li-O_2 batteries. The growth of ultrathin nanosheet-shaped discharge product on the 1D catalyst of Mn_3O_4 nanowires decorated with RuO_2 nanoparticles (Mn_3O_4-RuO_2) with intimate contact arises from the modulated electronic structure of RuO_2 for enhancing the adsorption ability of the LiO_2 intermediate, which enables that it can be smoothly decomposed under a low overpotential. Interestingly, a higher energy efficiency of 83% can be achieved at a high temperature of 55 °C. The present study demonstrates a simple yet efficient approach to configure the conductive and porous electrode with highly-dispersed catalyst for high-efficiency and long-life Li-O_2 batteries and paves a way for the design of highly effective catalyst for energy storage and conversion.

2. Experimental section

2.1. Material preparation

All reagents used in the present work were of analytical grade without further purification.

2.2. Synthesis of Mn_3O_4/CNTs-RuO_2 film

To synthesize MnOOH nanowires, 85 mg of $KMnO_4$ and 42 mg of polyvinylpyrrolidone (PVP, K30) were dissolved into 80 mL of deionized (DI) water under a continuous stirring for 30 min. Then, the solution was transferred into 120 mL of Teflon-line stainless-steel autoclave and kept 140 °C for 25 h. The MnOOH nanowires were yielded by several centrifugation and followed drying process. The CNTs used in this work were treated by acid oxidation. Typically, 0.2g of CNTs were dispersed into 60 mL of HNO_3 (69.2 wt%) by 60 min sonication. Then, the solution was transferred into 80 mL of Teflon-line stainless-steel autoclave and kept 100 °C for 1.5 h. After several centrifugation and followed drying processes, the surface-modified CNTs (m-CNTs) were yielded. The MnOOH/m-CNTs film, MnOOH film, and m-CNTs film were fabricated by the vacuum filtration of the mixed MnOOH and m-CNTs dispersed solution, pristine MnOOH dispersed solution, and pristine m-CNTs dispersed solution, respectively. After that, these films were annealed at 300 °C for 3 h in Ar atmosphere with a ramping rate of 2 °C min^{-1}, yielding the final product of Mn_3O_4/CNTs film, Mn_3O_4 film and CNTs film. The Mn_3O_4/CNTs-RuO_2 film was prepared by a typical atomic layer deposition process.

2.3. Materials characterization

The morphology and structure of the as-made samples were characterized with scanning electron microscopy (SEM, Hitachi S-4800) and transmission electron microscopy (TEM, FEI TF30). The composition and chemical state were measured by X-ray diffraction (XRD, Bruker D8 Advance, Cu K α X-ray source), Raman (HORIBA Scientific LabRAM HR) and X-ray photoelectron spectroscopy (XPS, Thermo ESCALAB 250). Thermo gravimetric analysis (TGA) was carried out on a TA SDT Q600 in an Air atmosphere from room temperature to 800 °C at a heating rate of 10 °C min^{-1}.

2.4. Electrochemical tests

Li-O_2 batteries performance tests were carried out by using meshed 2016-type coin cells. All electrodes adopted are free-standing without any auxiliary binder and conductive agent. Li-O_2 batteries were assembled in an argon-filled glove box (O_2 < 0.1 ppm and H_2O < 0.1 ppm) with tetraethylene glycol dimethyl ether (TEGDME) electrolyte containing 1 M LiTFSI. The electrochemical performance was measured using Arbin battery testing system in 1 atm O_2 at 25 °C. The cyclic voltammetry (CV) tests were performed on a Bio-Logic VSP electrochemical workstation within a voltage widow of 2.0–4.5 V at a scan rate of 0.2 mV s^{-1}.

3. Results and discussion

The Mn_3O_4/CNTs-RuO_2 film was prepared by a vacuum filtration coupled with ALD approach, as shown in Scheme 1. The morphology and structure of the free-standing Mn_3O_4, CNTs, Mn_3O_4/CNTs, and Mn_3O_4/CNTs-RuO_2 films were investigated by SEM and the typical images are shown in Fig. 1. As seen in Fig. 1a, the as-made Mn_3O_4 film features a highly interconnected and porous network architecture configured by 1D ultra-long Mn_3O_4 nanowires (Fig. S1). In contrast, a dense and agglomerated structure can be clearly seen in the Fig. 1b of the CNTs film SEM image, which is due to the flexible nature of 1D CNTs. As expected for the purpose of designing the advanced air electrode with developed pore structure and high conductivity, the Mn_3O_4/CNTs composite film was prepared. The SEM image in Fig. 1c reveals that Mn_3O_4 nanowires and CNTs are distributed uniformly throughout the composite film and the porous architecture derived from the skeleton effects of Mn_3O_4 nanowires are well inherited. The inset in Fig. 1c manifests that the as-made Mn_3O_4/CNTs film features the free-standing structure, which can be employed as the monolithic

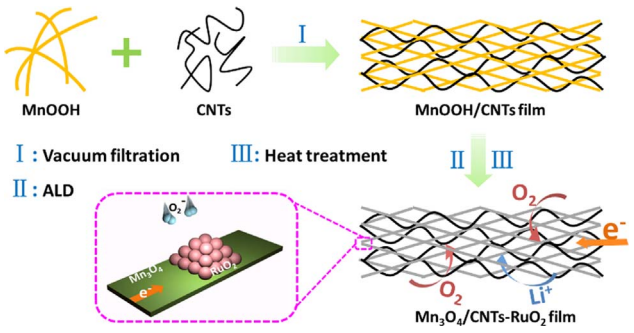

Scheme 1. Schematic illustration for the fabrication of Mn_3O_4/CNTs-RuO_2 film.

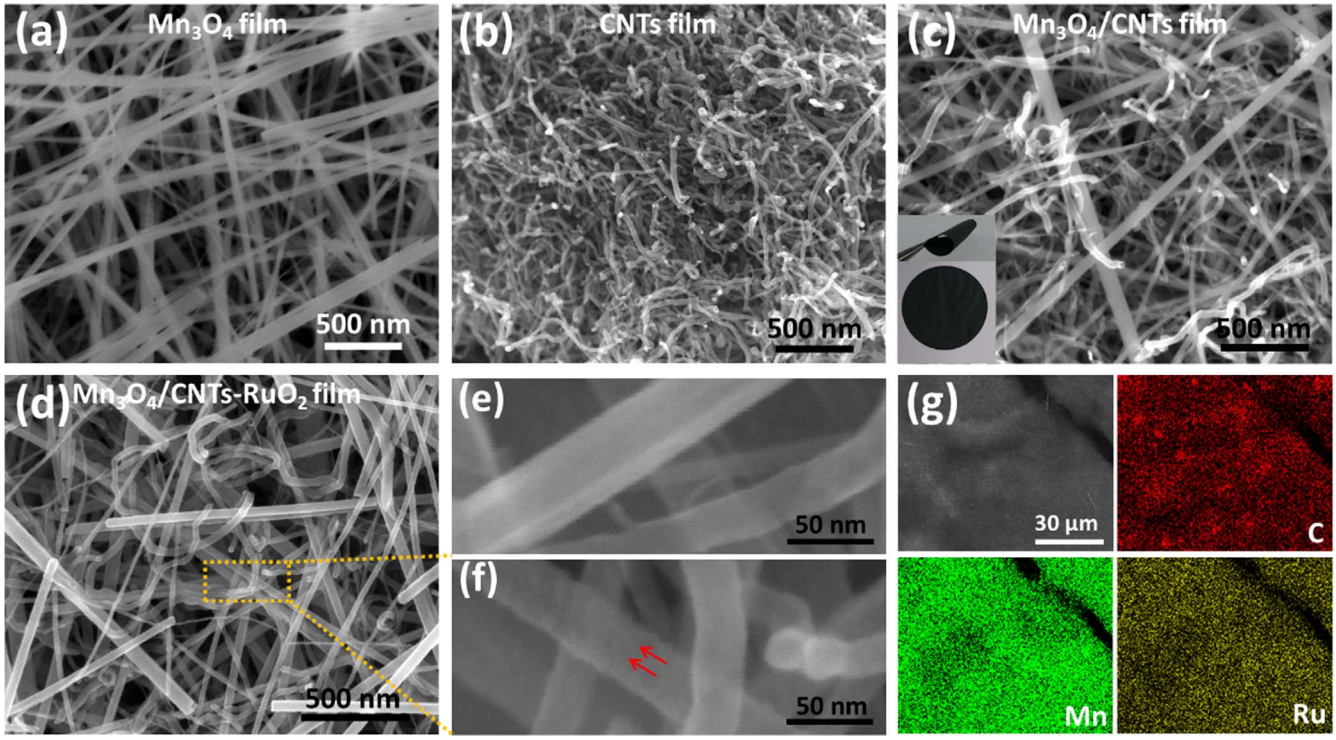

Fig. 1. SEM images of the (a) Mn_3O_4 film, (b) CNTs film, (c) Mn_3O_4/CNTs film, and (d) Mn_3O_4/CNTs-RuO_2 film, the inset in Fig. 1c: the digital photographs of the Mn_3O_4/CNTs film. The high-resolution SEM images of the (e) Mn_3O_4/CNTs film and (f) Mn_3O_4/CNTs-RuO_2 film. (g) SEM image of the Mn_3O_4/CNTs-RuO_2 film and the corresponding EDX elemental mapping images.

air electrode without any auxiliary binder and conductive agent [39]. After the deposition of RuO_2 nanoparticles by ALD process, the relatively loose and porous structure of Mn_3O_4/CNTs-RuO_2 film still can be retained, as shown in Fig. 1d. Meanwhile, the cross-section SEM image (Fig. S2) of the Mn_3O_4/CNTs-RuO_2 film clearly shows a hierarchical structure with an average thickness of ca. 8.5 μm. Compared with the smooth surface of Mn_3O_4 nanowires in Mn_3O_4/CNTs film (shown in Fig. 1e), it can be observed that tremendous ultrafine RuO_2 nanoparticles are uniformly fixed on Mn_3O_4 nanowires after ALD process (Fig. 1f). Moreover, the uniform distribution of Mn_3O_4 nanowires, CNTs and RuO_2 nanoparticles in the Mn_3O_4/CNTs-RuO_2 film matrix was also confirmed by the energy-dispersive X-ray spectroscopy (EDX) elemental mapping of C, Mn and Ru elements (shown in Fig. 1g).

The nanostructure of the Mn_3O_4/CNTs-RuO_2 film was further investigated by TEM. As shown in Fig. 2a, b and Fig. S3, S4, it can be clearly noted that RuO_2 nanoparticles are uniformly fixed on the surface of Mn_3O_4 nanowires with the intimate contact which is also a common feature of materials made by ALD [37,38]. The average particle size of RuO_2 was *ca*. 2.17 nm (Fig. 2c). The high-resolution TEM (HRTEM) was further employed to detect the local structure and composition of the as-made Mn_3O_4/CNTs-RuO_2 film, and the results were shown in Fig. 2d. It can be found that the backbone shows well-resolved spacing between adjacent fringes of 0.249 nm, corresponding to Mn_3O_4 (211) lattice spacing. The particles on the surface of Mn_3O_4 backbone present a clear lattice spacing of 0.225 nm which can be indexed to the (200) plane of RuO_2 phase.

The crystalline structure and composition of the as-made Mn_3O_4/CNTs-RuO_2 film were examined by XRD and Raman techniques. The typical diffraction peaks of Mn_3O_4, CNTs and RuO_2 can be distinctly observed from the XRD pattern of Mn_3O_4/CNTs-RuO_2 sample (Fig. 3a), indicative of the successful deposition of RuO_2 nanoparticles. Nevertheless, the Raman spectrum of the as-made Mn_3O_4/CNTs-RuO_2 film does not show the characteristic peaks of RuO_2 (Fig. 3b), suggesting extremely low amount of RuO_2 in the Mn_3O_4/CNTs-RuO_2 film matrix. The accurate content of RuO_2 in Mn_3O_4/CNTs-RuO_2 film was calculated to be as low as 2.84 wt% based on the Ru concentration by inductively coupled plasma atomic emission spectrometer (ICP-AES), which is consistent with the results of TEM and Raman characterizations. The surface chemical state of the as-made Mn_3O_4/CNTs-RuO_2 film was analyzed by XPS. The XPS survey spectrum shown in Fig. S6 confirms that the as-prepared sample mainly consists of C, O, Mn and Ru elements. According to the high-resolution Mn 2p XPS spectrum (Fig. 3c), two major characteristic peaks at 641.5 and 653.3 eV corresponding to the Mn $2p_{3/2}$ and Mn $2p_{1/2}$ of Mn_3O_4, respectively, can be clearly observed. Due to the very strong overlap between the Ru $3d_{3/2}$ and C 1 s regions as shown in Fig. 3d, the unoverlapped Ru $3d_{5/2}$ region is studied. Compared with the commercial RuO_2, the Ru $3d_{5/2}$ peak of Mn_3O_4/CNTs-RuO_2 film shows an obvious shift to high binding energy, corresponding to the transition to higher valence state, which may be attributed to its strong interaction with Mn_3O_4. In order to further confirm this assumption, the X-ray absorption (XAS) technique was employed to explore the valence change of Mn element in Mn_3O_4 after being grafted with RuO_2 nanoparticles (Fig. 4). It can be found from the Mn K-edge X-ray absorption near edge structure (XANES) spectra of the Mn_3O_4/CNTs film and Mn_3O_4/CNTs-RuO_2 film that the valence state of Mn in Mn_3O_4/CNTs-RuO_2 film shows a variation to low valence, indicating that electrons from RuO_2 nanoparticles have been transferred to Mn_3O_4, which is also consistent with the results of XPS above and reported in literature [40]. The RuO_2 with electron deficiency may possess stronger adsorption ability to the electron-rich O_2^- or LiO_2 than that of the normal RuO_2, which will bound the chemical disproportionation reactions of LiO_2 happened on the surface of catalysts rather than in the electrolyte [41–43]. In view of the uniquely structural and compositional characteristics mentioned above, it is expected that the as-made Mn_3O_4/CNTs-RuO_2 film would be capable of being excellent air electrodes for Li-O_2 batteries.

The electrochemical performance of the as-made Mn_3O_4/CNTs-RuO_2 film was evaluated by using 2016-type coin cells with a Li metal anode, an electrolyte of 1 M LiTFSI in TEGDME and a slice of Mn_3O_4/

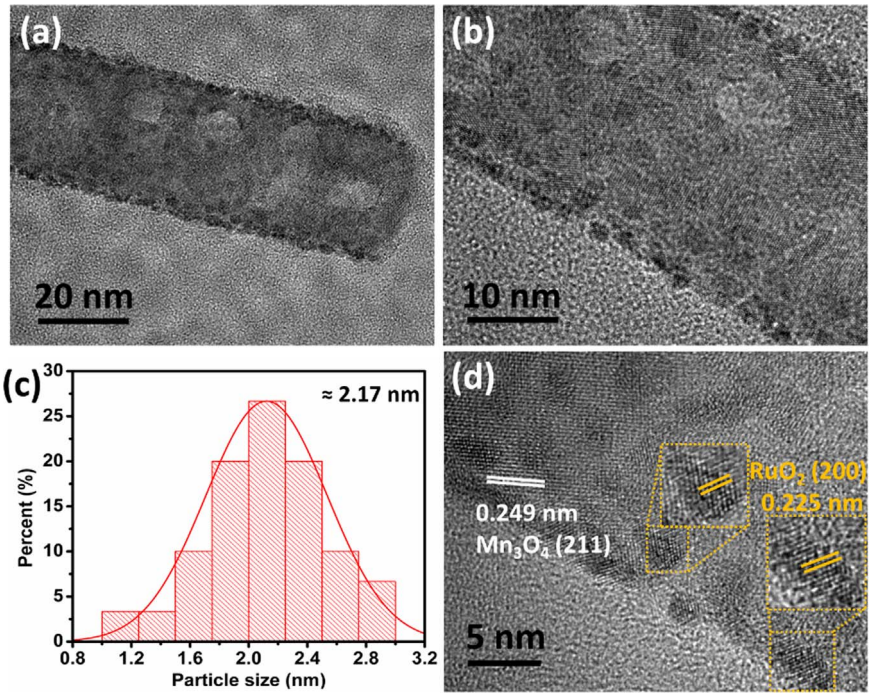

Fig. 2. (a, b) TEM images of the Mn_3O_4/CNTs-RuO_2 film. (c) The histograms of RuO_2 particle size distribution. (d) HRTEM image of the Mn_3O_4/CNTs-RuO_2 film.

CNTs-RuO_2 film. Fig. 5a shows the CV curves of the as-made samples within a voltage window of 2.0–4.5 V at a scan rate of 0.2 mV s^{-1}. It can be clearly seen that the Mn_3O_4/CNTs-RuO_2 film and Mn_3O_4/CNTs film deliver the same onset potential and peak current during discharge process, and far outperform these of the Mn_3O_4 film and CNTs film. More importantly, compared with the Mn_3O_4/CNTs film, the Mn_3O_4/CNTs-RuO_2 film can achieve a lower onset potential and higher peak current upon charge due to the highly catalytic activity of RuO_2 [44,45]. The electro-catalytic performance of the as-prepared Mn_3O_4/CNTs-RuO_2 film was also examined by galvanostatic discharge-charge measurement at a current density of 100 mA g^{-1}. Fig. 5b reveals that the Mn_3O_4/CNTs-RuO_2 film delivers the highest discharge specific capacity of 7198 mA h g^{-1} than that of Mn_3O_4/CNTs film (6236 mA h g^{-1}), CNTs film (829 mA h g^{-1}) and Mn_3O_4 film (9 mA h g^{-1}), highlighting the advantages of the interconnected porous structure and high conductivity [46]. Interestingly, the Mn_3O_4/CNTs-RuO_2 film displays an evidently lower overpotential than that of Mn_3O_4/CNTs film upon the charge process, indicative of the outstanding OER catalytic activity in Li-O_2 batteries, which is also consistent with the CV results discussed above. Inspired by this, we

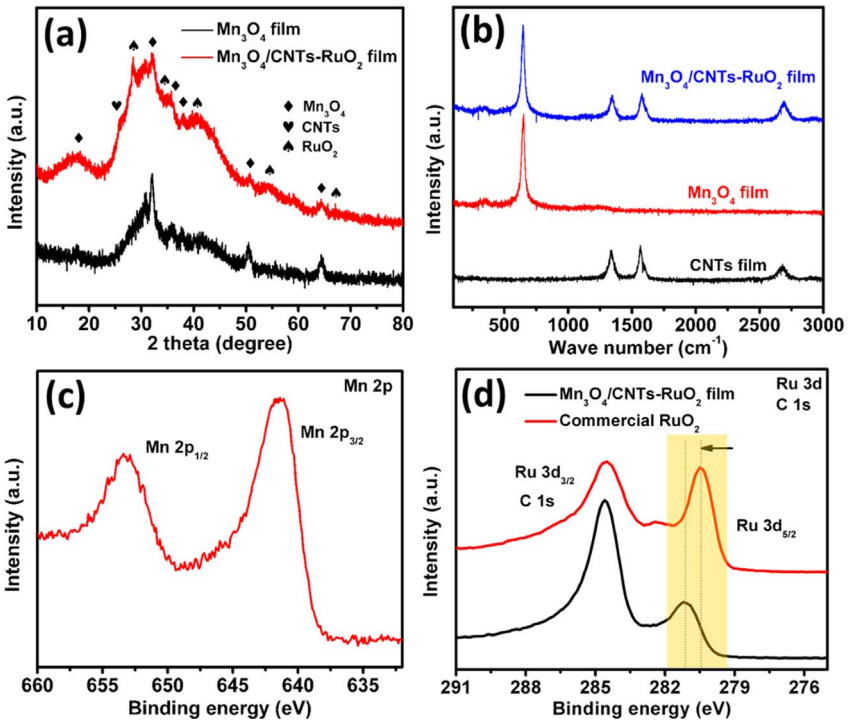

Fig. 3. (a) XRD patterns of the Mn_3O_4 film and Mn_3O_4/CNTs-RuO_2 film. (b) Raman spectra of the CNTs film, Mn_3O_4 film, and Mn_3O_4/CNTs-RuO_2 film. (c) Mn 2p XPS spectrum of the Mn_3O_4/CNTs-RuO_2 film. (d) Ru 3d XPS spectra of the Mn_3O_4/CNTs-RuO_2 film and commercial RuO_2.

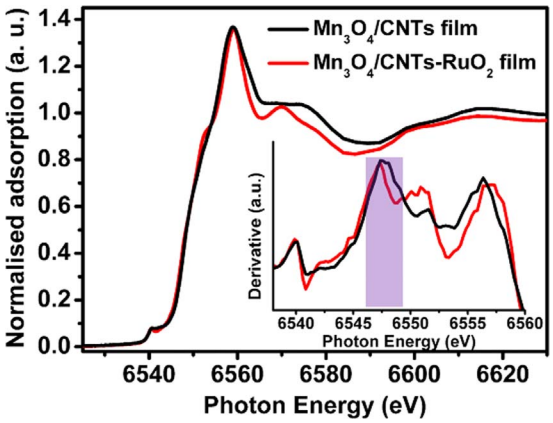

Fig. 4. Normalized XANES spectra of Mn K-edge for the Mn_3O_4/CNTs film and Mn_3O_4/CNTs-RuO_2 film, the inset: the corresponding derivative normalized XANES spectra.

further examined the energy efficiency of the Mn_3O_4/CNTs-RuO_2 film by the galvanostatic discharge-charge process with a fixed capacity of 700 mA h g^{-1}, and the result is shown in Fig. 5c. The Mn_3O_4/CNTs-RuO_2 film exhibits a high discharge voltage (2.85 V) and a low charge voltage (3.70 V), corresponding to an energy efficiency of 77.8% which is much higher than that of the Mn_3O_4/CNTs film. These results indicate the as-prepared Mn_3O_4/CNTs-RuO_2 film is an efficient catalyst for OER process in aprotic Li-O_2 batteries. The cycling stability of Li-O_2 batteries is another severe concern for practical applications. In this case, the cycling performance measurement was performed at a current density of 200 mA g^{-1} with a fixed capacity of 700 mA h g^{-1} of which the results are shown in Fig. 5d. It can be seen that the as-made Mn_3O_4/CNTs-RuO_2 film can be cycled 251 cycles with no capacity loss, which is superior to that of Mn_3O_4/CNTs film (49 cycles). More importantly, the terminal charge voltage of Mn_3O_4/CNTs-RuO_2 film electrode can be kept as low as 4.1 V among the first 200 cycles, indicative of the complete decomposition of discharge product at reduced overpotentials. The corresponding discharge-charge profiles (Fig. 5e) further reveal that the Li-O_2 batteries with the Mn_3O_4/CNTs-RuO_2 film can be run more than 1700 h without degradation, further highlighting the excellent catalysis effect of ALD RuO_2. Moreover, compared with the Ru-based catalyst reported in previous literature, it can be found that the as-made Mn_3O_4/CNTs-RuO_2 film herein requires the lowest amount of RuO_2 and is also among the best performance in the reported Ru-based catalyst as air electrode for Li-O_2 batteries (Table S1).

The morphology and structure of the Mn_3O_4/CNTs-RuO_2 film after discharge and recharge were further examined by SEM, and the results are shown in Fig. 6. It can be clearly seen that a large amount of micron-scale sheet-shaped discharge product was embedded in the matrix of Mn_3O_4/CNTs-RuO_2 film after full discharge (Fig. 6a). Interestingly, after fully recharge, the electrode can almost recover to its original structure (Fig. 6b), indicative of the complete decomposition of the discharge product. The composition of the discharge product was further analyzed by XRD and Fourier transform infrared (FTIR) spectroscopy, of which the detailed results are shown in Fig. 6c and Fig. S9, respectively. It can be noted that Li_2O_2 is the main discharge product and almost disappears after recharge. The reversible formation and decomposition of the discharge product reveal the high electro-catalytic activity of the Mn_3O_4/CNTs-RuO_2 film [47,48]. In contrast, it can be noted from the SEM image in Fig. S10 that the discharge product of Mn_3O_4/CNTs film electrode was described in the typical toroid-like structure [49]. In order to further explore the reason for excellent cycling stability of Li-O_2 batteries with the Mn_3O_4/CNTs-RuO_2 film, the morphology of the Mn_3O_4/CNTs-RuO_2 film electrode after partly discharge was investigated, and the results are shown in Fig. 6d–f. It can be found that the ultrathin nanosheet-shaped discharge product was deposited on the Mn_3O_4-RuO_2 catalyst keeping an intimate contact between them, which is attributed to

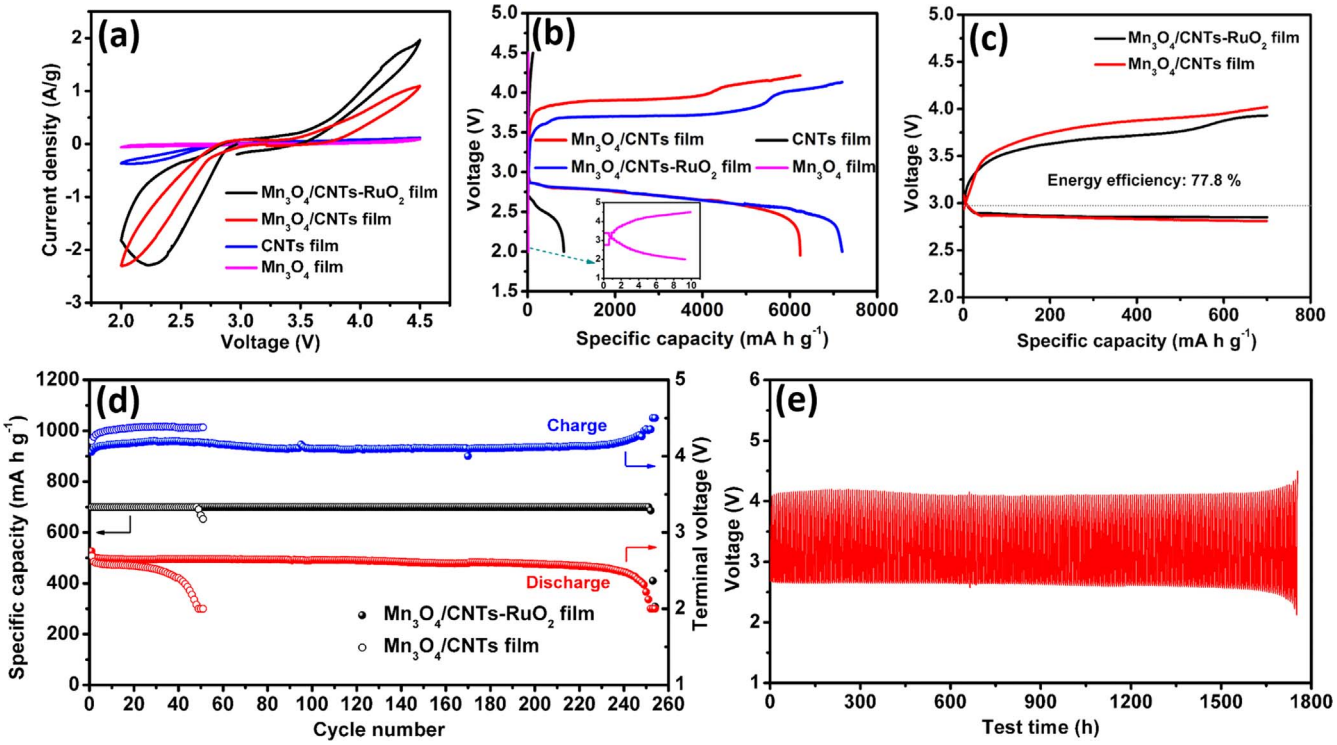

Fig. 5. (a) CV curves of the as-made samples within a voltage widow of 2.0–4.5 V at a scan rate of 0.2 mV s^{-1}. (b) The initial discharge-charge profiles of Li-O_2 batteries based on the as-made samples at a current density of 100 mA g^{-1}, the inset: the magnified initial discharge-charge profiles of Li-O_2 batteries based on the Mn_3O_4 film. (c) The initial discharge-charge profiles of Li-O_2 batteries based on the Mn_3O_4/CNTs film and Mn_3O_4/CNTs-RuO_2 film at a current density of 100 mA g^{-1} with a fixed capacity of 700 mA h g^{-1}. (d) Discharge capacity and the discharge and charge terminal voltage versus the cycle number for Li-O_2 batteries based on the Mn_3O_4/CNTs film and Mn_3O_4/CNTs-RuO_2 film at a current density of 200 mA g^{-1}. (e) The discharge-charge profiles of Li-O_2 batteries based on the Mn_3O_4/CNTs-RuO_2 film at a current density of 200 mA g^{-1} with a fixed capacity of 700 mA h g^{-1}.

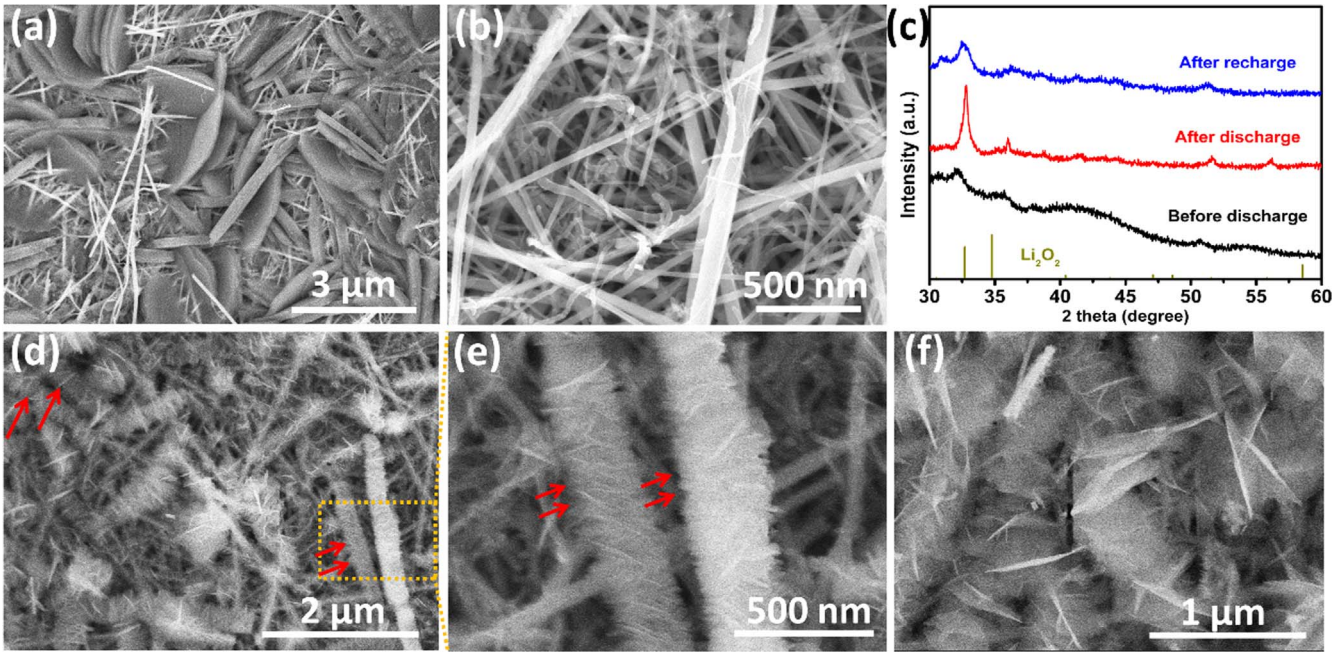

Fig. 6. SEM images of the Mn_3O_4/CNTs-RuO_2 film after (a) full discharge and (b) full recharge. (c) XRD patterns of the Mn_3O_4/CNTs-RuO_2 film at different discharge-charge states. (d–f) SEM images of the Mn_3O_4/CNTs-RuO_2 film after partly discharge.

the modulated electronic structure of RuO_2 for enhancing the adsorption ability of the intermediate of LiO_2 [50,51]. In this case, the chemical disproportionation reactions of LiO_2 were confined to take place on the surface of catalysts rather than in the electrolyte, avoiding to form the large compact toroid-like discharge product particles [52,53]. The uniformly distributed RuO_2 nanoparticles catalytically serve as the active sites and nucleation sites for the growth of nanosheet-shaped discharge product. As a result, the discharge product can be smoothly decomposed under a low overpotential, leading to an excellent cycling stability.

In addition, the batteries with Mn_3O_4/CNTs-RuO_2 air electrode were tested at a relatively high temperature of 55 °C in order to further enhance their energy efficiency. The results are shown in Fig. 7. As seen from the CV curves of the Mn_3O_4/CNTs-RuO_2 film tested at different temperature (Fig. 7a), an obviously enhanced OER catalytic activity can be achieved at the high temperature, evidenced by a lower charge onset and higher charge peak current. Fig. 7b demonstrates at an increased temperature of 55 °C, the battery exhibits a significantly reduced charge voltage of 3.5 V, delivering a higher energy efficiency up to 83% than room temperature. Therefore, this will be a simple and efficient strategy for enhancing the energy efficiency of Li-O_2 batteries. Further works about the regarding using ALD catalyst for high temperature Li-O_2 batteries will be ongoing.

4. Conclusion

In summary, the free-standing Mn_3O_4/CNTs-RuO_2 film has been rationally designed and successfully prepared by a vacuum filtration coupled with ALD method, and evaluated its electrochemical performance as a binder-free air electrode for Li-O_2 batteries. The Mn_3O_4/CNTs composite film is constructed as a well-interconnected conductive substrate based on the skeleton role of Mn_3O_4 nanowires and the excellent conductor role of CNTs. The ALD method was employed to controllably deposit uniformly dispersed and extremely low amount of RuO_2 nanoparticles (2.84 wt%) as for superior OER catalyst. As a result, the free-standing Mn_3O_4/CNTs-RuO_2 film electrode delivers a high specific capacity, high energy efficiency and long cycle stability up to 251 cycles, which is attributed to the reversible formation and decomposition of the ultrathin nanosheet-shaped discharge product. The backbone of Mn_3O_4 can modulate the electronic structure of RuO_2 for enhancing the adsorption ability of the intermediate of LiO_2 and further forming the nanosheet-shaped discharge product. Moreover, a further enhanced energy efficiency of 83% can be achieved at a relatively high temperature. The present study demonstrates a simple yet efficient approach to configuring the conductive and porous electrode with highly-dispersed catalyst for high-efficiency and long-life Li-O_2 batteries and paves one's way for the design of highly effective

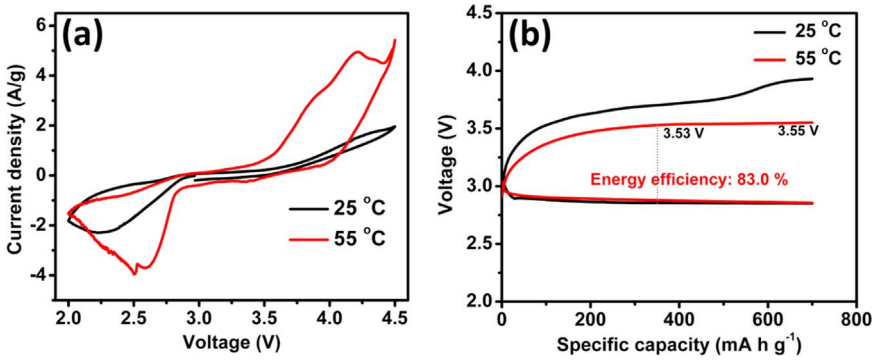

Fig. 7. (a) CV curves of the Mn_3O_4/CNTs-RuO_2 film at different temperature within a voltage widow of 2.0–4.5 V at a scan rate of 0.2 mV s^{-1}. (b) The discharge-charge profiles of Mn_3O_4/CNTs-RuO_2 film at different temperature with a fixed capacity of 700 mA h g^{-1} at the current density of 100 mA g^{-1}.

catalyst for energy storage and conversion devices.

Acknowledgements

C. Zhao and C. Yu contributed equally to this work. This work was partly supported by the National Natural Science Foundation of China (NSFC, nos. 21361162004 and 21522601), the Education Department of the Liaoning Province of China (No. T2013001), Natural Sciences and Engineering Research Council of Canada (NSERC), Canada Research Chair Program (CRC), Canada Foundation for Innovation (CFI), Ontario Research Fund (ORF), the University of Western Ontario, and Canada Light Source. C. Zhao was supported by the Chinese Scholarship Council.

Appendix A. Supplementary material

Supplementary data associated with this article can be found in the online version at http://dx.doi.org/10.1016/j.nanoen.2017.02.030.

References

[1] P.G. Bruce, S.A. Freunberger, L.J. Hardwick, J.-M. Tarascon, Nat. Mater. 11 (2012) 19–29.
[2] Y.-C. Lu, B.M. Gallant, D.G. Kwabi, J.R. Harding, R.R. Mitchell, M.S. Whittingham, Y. Shao-Horn, Energy Environ. Sci. 6 (2013) 750–768.
[3] T. Liu, M. Leskes, W. Yu, A.J. Moore, L. Zhou, P.M. Bayley, G. Kim, C.P. Grey, Science 350 (2015) 530–533.
[4] J. Lu, Y. Jung Lee, X. Luo, K. Chun Lau, M. Asadi, H.-H. Wang, S. Brombosz, J. Wen, D. Zhai, Z. Chen, D.J. Miller, Y. Sub Jeong, J.-B. Park, Z. Zak Fang, B. Kumar, A. Salehi-Khojin, Y.-K. Sun, L.A. Curtiss, K. Amine, Nature 529 (2016) 377–382.
[5] S. Ma, Y. Wu, J. Wang, Y. Zhang, Y. Zhang, X. Yan, Y. Wei, P. Liu, J. Wang, K. Jiang, S. Fan, Y. Xu, Z. Peng, Nano Lett. 15 (2015) 8084–8090.
[6] Y.-C. Lu, Z. Xu, H.A. Gasteiger, S. Chen, K. Hamad-Schifferli, Y. Shao-Horn, J. Am. Chem. Soc. 132 (2010) 12170–12171.
[7] G. Zhao, R. Mo, B. Wang, L. Zhang, K. Sun, Chem. Mater. 26 (2014) 2551–2556.
[8] E. Yilmaz, C. Yogi, K. Yamanaka, T. Ohta, H.R. Byon, Nano Lett. 13 (2013) 4679–4684.
[9] J. Xie, Q. Dong, I. Madden, X. Yao, Q. Cheng, P. Dornath, W. Fan, D. Wang, Nano Lett. 15 (2015) 8371–8376.
[10] J. Xiao, D. Mei, X. Li, W. Xu, D. Wang, G.L. Graff, W.D. Bennett, Z. Nie, L.V. Saraf, I.A. Aksay, J. Liu, J.-G. Zhang, Nano Lett. 11 (2011) 5071–5078.
[11] W.-H. Ryu, T.-H. Yoon, S.H. Song, S. Jeon, Y.-J. Park, I.-D. Kim, Nano Lett. 13 (2013) 4190–4197.
[12] W.-H. Ryu, F.S. Gittleson, M. Schwab, T. Goh, A.D. Taylor, Nano Lett. 15 (2015) 434–441.
[13] H.-D. Lim, K.-Y. Park, H. Song, E.Y. Jang, H. Gwon, J. Kim, Y.H. Kim, M.D. Lima, R.O. Robles, X. Lepró, R.H. Baughman, K. Kang, Adv. Mater. 25 (2013) 1348–1352.
[14] Q. Li, P. Xu, W. Gao, S. Ma, G. Zhang, R. Cao, J. Cho, H.-L. Wang, G. Wu, Adv. Mater. 26 (2014) 1378–1386.
[15] Z. Guo, D. Zhou, X. Dong, Z. Qiu, Y. Wang, Y. Xia, Adv. Mater. 25 (2013) 5668–5672.
[16] B. Sun, S. Chen, H. Liu, G. Wang, Adv. Funct. Mater. 25 (2015) 4436–4444.
[17] Y. Yang, W. Yin, S. Wu, X. Yang, W. Xia, Y. Shen, Y. Huang, A. Cao, Q. Yuan, ACS Nano 10 (2016) 1240–1248.
[18] D. Oh, J. Qi, Y.-C. Lu, Y. Zhang, Y. Shao-Horn, A.M. Belcher, Nat. Commun. 4 (2013).
[19] H. Wang, Y. Yang, Y. Liang, G. Zheng, Y. Li, Y. Cui, H. Dai, Energy Environ. Sci. 5 (2012) 7931–7935.
[20] J. Park, Y.-S. Jun, W.-r. Lee, J.A. Gerbec, K.A. See, G.D. Stucky, Chem. Mater. 25 (2013) 3779–3781.
[21] H.-D. Lim, H. Song, J. Kim, H. Gwon, Y. Bae, K.-Y. Park, J. Hong, H. Kim, T. Kim, Y.H. Kim, X. Lepró, R. Ovalle-Robles, R.H. Baughman, K. Kang, Angew. Chem. Int. Ed. 53 (2014) 3926–3931.
[22] Z. Zhang, J. Bao, C. He, Y. Chen, J. Wei, Z. Zhou, Adv. Funct. Mater. 24 (2014) 6826–6833.
[23] L. Liu, J. Wang, Y. Hou, J. Chen, H.-K. Liu, J. Wang, Y. Wu, Small 12 (2016) 602–611.
[24] J. Zhang, Y. Zhao, X. Zhao, Z. Liu, W. Chen, Sci. Rep. 4 (2014) 6005.
[25] S.H. Oh, R. Black, E. Pomerantseva, J.-H. Lee, L.F. Nazar, Nat. Chem. 4 (2012) 1004–1010.
[26] D. Sun, Y. Shen, W. Zhang, L. Yu, Z. Yi, W. Yin, D. Wang, Y. Huang, J. Wang, D. Wang, J.B. Goodenough, J. Am. Chem. Soc. 136 (2014) 8941–8946.
[27] J.-L. Shui, N.K. Karan, M. Balasubramanian, S.-Y. Li, D.-J. Liu, J. Am. Chem. Soc. 134 (2012) 16654–16661.
[28] S.-M. Xu, Q.-C. Zhu, J. Long, H.-H. Wang, X.-F. Xie, K.-X. Wang, J.-S. Chen, Adv. Funct. Mater. 26 (2016) 1365–1374.
[29] K.R. Yoon, G.Y. Lee, J.-W. Jung, N.-H. Kim, S.O. Kim, I.-D. Kim, Nano Lett. 16 (2016) 2076–2083.
[30] Y.S. Jeong, J.-B. Park, H.-G. Jung, J. Kim, X. Luo, J. Lu, L. Curtiss, K. Amine, Y.-K. Sun, B. Scrosati, Y.J. Lee, Nano Lett. 15 (2015) 4261–4268.
[31] P. Tan, Z.H. Wei, W. Shyy, T.S. Zhao, X.B. Zhu, Energy Environ. Sci. 9 (2016) 1783–1793.
[32] Z. Jian, P. Liu, F. Li, P. He, X. Guo, M. Chen, H. Zhou, Angew. Chem. Int. Ed. 53 (2014) 442–446.
[33] X. Huang, H. Yu, H. Tan, J. Zhu, W. Zhang, C. Wang, J. Zhang, Y. Wang, Y. Lv, Z. Zeng, D. Liu, J. Ding, Q. Zhang, M. Srinivasan, P.M. Ajayan, H.H. Hng, Q. Yan, Adv. Funct. Mater. 24 (2014) 6516–6523.
[34] H.-G. Jung, Y.S. Jeong, J.-B. Park, Y.-K. Sun, B. Scrosati, Y.J. Lee, ACS Nano 7 (2013) 3532–3539.
[35] W.-B. Luo, S.-L. Chou, J.-Z. Wang, Y.-C. Zhai, H.-K. Liu, Small 11 (2015) 2817–2824.
[36] X. Han, Y. Hu, J. Yang, F. Cheng, J. Chen, Chem. Commun. 50 (2014) 1497–1499.
[37] Y. Lei, J. Lu, X. Luo, T. Wu, P. Du, X. Zhang, Y. Ren, J. Wen, D.J. Miller, J.T. Miller, Y.-K. Sun, J.W. Elam, K. Amine, Nano Lett. 13 (2013) 4182–4189.
[38] K.E. Gregorczyk, A.C. Kozen, X. Chen, M.A. Schroeder, M. Noked, A. Cao, L. Hu, G.W. Rubloff, ACS Nano 9 (2015) 464–473.
[39] S. Liu, Y. Zhu, J. Xie, Y. Huo, H.Y. Yang, T. Zhu, G. Cao, X. Zhao, S. Zhang, Adv. Energy Mater. 4 (2014) 1301960.
[40] B. Zhang, J. Chen, P. Yang, X. Chi, W. Lin, T. Venkatesan, C.-J. Sun, S.M. Heald, G.M. Chow, Sci. Rep. 6 (2016) 19886.
[41] L. Johnson, C. Li, Z. Liu, Y. Chen, S.A. Freunberger, P.C. Ashok, B.B. Praveen, K. Dholakia, J.-M. Tarascon, P.G. Bruce, Nat. Chem. 6 (2014) 1091–1099.
[42] S. Dong, S. Wang, J. Guan, S. Li, Z. Lan, C. Chen, C. Shang, L. Zhang, X. Wang, L. Gu, G. Cui, L. Chen, J. Phys. Chem. Lett. 5 (2014) 615–621.
[43] L. Shi, A. Xu, T. Zhao, J. Phys. Chem. C 120 (2016) 6356–6362.
[44] F. Li, Y. Chen, D.-M. Tang, Z. Jian, C. Liu, D. Golberg, A. Yamada, H. Zhou, Energy Environ. Sci. 7 (2014) 1648–1652.
[45] X. Guo, P. Liu, J. Han, Y. Ito, A. Hirata, T. Fujita, M. Chen, Adv. Mater. 27 (2015) 6137–6143.
[46] J. Shui, F. Du, C. Xue, Q. Li, L. Dai, ACS Nano 8 (2014) 3015–3022.
[47] Y.-B. Yin, J.-J. Xu, Q.-C. Liu, X.-B. Zhang, Adv. Mater. 28 (2016) 7494–7500.
[48] C. Zhao, C. Yu, S. Liu, J. Yang, X. Fan, H. Huang, J. Qiu, Adv. Funct. Mater. 25 (2015) 6913–6920.
[49] S. Lau, L.A. Archer, Nano Lett. 15 (2015) 5995–6002.
[50] R. Choi, J. Jung, G. Kim, K. Song, Y.-I. Kim, S.C. Jung, Y.-K. Han, H. Song, Y.-M. Kang, Energy Environ. Sci. 7 (2014) 1362–1368.
[51] X. Lu, J. Deng, W. Si, X. Sun, X. Liu, B. Liu, L. Liu, S. Oswald, S. Baunack, H.J. Grafe, C. Yan, O.G. Schmidt, Adv. Sci. 2 (2015) 1500113.
[52] C. Shang, S. Dong, P. Hu, J. Guan, D. Xiao, X. Chen, L. Zhang, L. Gu, G. Cui, L. Chen, Sci. Rep. 5 (2015) 8335.
[53] P. Zhang, R. Wang, M. He, J. Lang, S. Xu, X. Yan, Adv. Funct. Mater. 26 (2016) 1354–1364.

Changtai Zhao is currently a Ph.D. candidate in Prof. Jieshan Qiu's group at Dalian University of Technology, China. He was also a visiting student in Prof. Xueliang (Andy) Sun's Group at the University of Western Ontario, Canada, in 2016. He gained his Bachelor's degree from Department of Chemical Engineering, Qingdao University, China. His research interests focus on nanocarbon and advanced functional materials as well as their applications in energy conversion and storage, especially for Na/Li-ion batteries, Li-S batteries and Li-O_2 batteries.

Prof. Chang Yu received her Ph.D. degree from the School of Chemical Engineering at Dalian University of Technology (DUT) in 2008. She is currently a professor for School of Chemical Engineering at DUT. She was also a visiting professor at Rice University (USA) in 2015. Her research interests mainly focus on carbon coupled two-dimensional inorganic layered materials for energy storage and conversion applications.

Dr. Mohammad Norouzi Banis is research engineer in Prof. Xueliang (Andy) Sun's at University of Western Ontario, Canada. He received his Ph.D. degree in 2013 in Materials Science and Engineering from Western University, on the study of nanostructured low temperature fuel cells and application of x-ray absorption spectroscopy in energy related systems. His current research interests include study of metal ion, metal air and nanocatalysts via in-situ synchrotron based techniques.

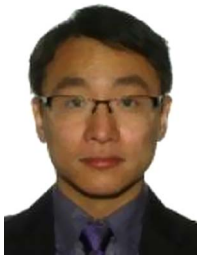

Dr. Qian Sun is a postdoctoral fellow in Prof. Xueliang (Andy) Sun's Group at the University of Western Ontario, Canada. He received his B.S. degree in Chemistry in 2006, M.S. degree in Physical Chemistry in 2009, and Ph.D. degree in Applied Chemistry in 2013 at Fudan University, China, under the supervision of Prof. Dr. Zheng-Wen Fu on the study of Li-/Na-ion batteries and Na-air batteries. He joined Prof. Sun's group in 2013 and his current research interests focus on Na-air, Na-S, and Na-ion batteries as well as solid-state Li/Na batteries.

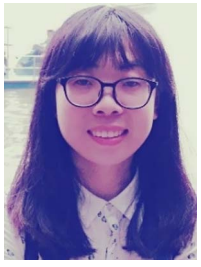

Mengdi Zhang received her B.S. degree in Chemical Technology from Dalian University of Technology in 2012. Currently, she is a Ph.D. candidate at School of Chemical Engineering in Dalian University of Technology under the supervision of Prof. Jieshan Qiu. Her research mainly focuses on the design and synthesis of carbon-based nanomaterials for the application in supercapacitor and lithium secondary batteries.

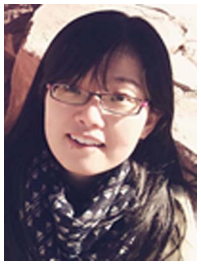

Xia Li is currently a Ph.D. candidate in Prof. Xueliang (Andy) Sun's Nanomaterials and Energy Group at the University of Western Ontario, Canada. She received her Bachelor degree at Dalian University of Technology, China, and Master degree at Nankai University, China. Her current research interests focus on development of advanced nanomaterials for lithium-sulfur batteries

Yulong Liu is currently a Ph.D. candidate in Prof. Xueliang (Andy) Sun' Nanomaterials and Energy Group at the University of Western Ontario, Canada. He received his Bachelor degree from Central South University, China, in 2010, and Master degree in 2013. His research interests include nanomaterials for lithium ion batteries, especially $LiFePO_4$ (in collaboration with *Phostech Lithium Inc.*), and the development of the solid state batteries.

Yang Zhao is currently a Ph.D. candidate in Prof. Xueliang (Andy) Sun's Group at the University of Western Ontario, Canada. He received his B.S. degree and M.S. degree in Chemical Engineering and Technology from Northwestern Polytechnical University (Xi'an, China) in 2011 and 2014, respectively. His current research interests focus on atomic layer deposition in the application of lithium/sodium ion batteries and all solid state batteries.

Huawei Huang received his B.S. degree from the Department of Materials Science and Engineering, Northeast Forestry University. Currently, he is a Ph.D. candidate at School of Chemical Engineering in Dalian University of Technology under the supervision of Prof. Jieshan Qiu. His research focuses on the synthesis of carbon-based nanomaterials and related functional materials for the applications in water splitting.

Shaofeng Li received his Bachelor's degree from the School of Chemistry and Chemical Engineering at Anhui University of Technology in 2014. He is currently a 1st year Ph.D. candidate in research group of Prof. Jieshan Qiu at Dalian University of Technology. His research interests mainly focus on rational design and optimization of carbon-based nanohybrids for energy storage and conversion application.

Xiaotong Han is a Ph.D. student in Prof. Jieshan Qiu's group at Dalian University of Technology (DUT), China. He received his B.S. degree in Chemical Engineering and Technology in 2013 at Nanjing Tech University, China. He joined Prof. Qiu's group in 2013 and his current research interests focus on the design and fabrication of two-dimension nanohybrids derived from nanocarbons and transition metal compounds for energy storage and conversion devices including Li-ion batteries, supercapacitors as well as electrocatalysis.

Dr. Biwei Xiao has just finished his Ph.D. degree in Prof. Xueliang (Andy) Sun's group at the University of Western Ontario. He earned his bachelor of engineering degree from Sichuan University (China) in 2011. His research interests are associated with the synthesis, modification and mechanism study of cathode materials for lithium-ion batteries, atomic layer deposition, synchrotron radiation technique and carbonaceous materials.

Zhongxin Song received her Master degree in Polymer Chemistry and Physics from Qingdao University of Science and Technology (China) in 2014. She is currently a Ph.D. student supervised by Prof. Xueliang (Andy) Sun in the University of Western Ontario, Canada. Currently, her focus is on development of novel nanomaterials as electrocatalysis and catalyst support in fuel cells.

Dr. Ruying Li is a research engineer at Prof. Xueliang (Andy) Sun's Nanomaterial and Energy Group at the University of Western Ontario, Canada. She received her master degree in Material Chemistry under the direction of Prof. George Thompson in 1999 at University of Manchester, UK, followed by work as a research assistant under the direction of Prof. Keith Mitchell at the University of British Columbia and under the direction of Prof. Jean-Pol Dodelet at I'Institut national de la recherché scientifique (INRS), Canada. Her current research interests are associated with synthesis and characterization of nanomaterials for electrochemical energy storage and conversion.

Prof. Jieshan Qiu obtained his Ph.D. degree in the School of Chemical Engineering at Dalian University of Technology (DUT) in 1990. He was also a visiting professor at Pennsylvania State University (USA), West Virginia University (USA), and the University of Reading (UK). He was appointed to a Cheung-Kong Distinguished Professor in 2009. He is a professor of School of Chemical Engineering and director of the Carbon Research Laboratory at DUT. His current research includes functional carbon nanotubes, graphene, carbon nanohybrids, and their applications (energy conversion and storage, capacitive deionization technique, etc.).

Prof. Xueliang (Andy) Sun is a Canada Research Chair in Development of Nanomaterials for Clean Energy, Fellow of the Royal Society of Canada and Canadian Academy of Engineering and Full Professor at the University of Western Ontario, Canada. Dr. Sun received his Ph.D. in materials chemistry in 1999 from the University of Manchester, UK, which he followed up by working as a postdoctoral fellow at the University of British Columbia, Canada and as a Research Associate at L'Institut National de la Recherche Scientifique (INRS), Canada. His current research interests are focused on advanced materials for electrochemical energy storage and conversion, including electrocatalysis in fuel cells and electrodes in lithium-ion batteries and metal-air batteries.